

TECHNICAL REVIEW

NO. 1 – 2016



Flight Test Validation of Noise Models for High Performance Military Aircraft
Using Beamforming

Use of a Portable Flanged Impedance Tube for Absorber Design and
Measurement

Brüel & Kjær 

BEYOND MEASURE

Previously issued numbers of Brüel & Kjær Technical Review

- 1 – 2015 Fast Wideband Acoustical Holography
Evaluation of SPC and BSS for Indoor Pass-by Noise Contribution Analysis
 - 1 – 2014 Experimental Characterization of Operating Bladed Rotor Using HPS and
SSI Techniques
Microphone Acoustic Impedance in Reciprocity Calibration
 - 1 – 2013 Noise Test of Revised Notched Nozzle Using a Jet Engine
Heat Conduction Correction in Reciprocity Calibration of Laboratory
Standard Microphones
 - 1 – 2012 High-resolution Fly-over Beamforming
Clustering Approaches to Automatic Modal Parameter Estimation
 - 1 – 2011 Performance Investigation of the Dual-Layer Array (DLA) at Low
Frequencies
Calculating the Sound Field in an Acoustic Intensity Probe Calibrator
– A Practical Utilisation of Boundary Element Modelling
Multi-field Microphone – When the Sound Field is Unknown
 - 1 – 2010 Time Selective Response Measurements – Good Practices and Uncertainty
Measurement of Absorption Coefficient, Radiated and Absorbed Intensity
on the Panels of a Vehicle Cabin using a Dual Layer Array with Integrated
Position Measurement
ISO 16063 – 11: Uncertainties in Primary Vibration Calibration by Laser
Interferometry – Reference Planes and Transverse Motion
 - 1 – 2009 Use of Volume Velocity Sound Sources in the Measurement of Acoustic
Frequency Response Functions
Turnkey Free-field Reciprocity System for Primary Microphone Calibration
 - 1 – 2008 ISO 16063–11: Primary Vibration Calibration by Laser Interferometry:
Evaluation of Sine Approximation Realised by FFT
Infrasound Calibration of Measurement Microphones
Improved Temperature Specifications for Transducers with Built-in
Electronics
 - 1 – 2007 Measurement of Normal Incidence Transmission Loss and Other Acoustical
Properties of Materials Placed in a Standing Wave Tube
 - 1 – 2006 Dyn-X Technology: 160 dB in One Input Range
Order Tracking in Vibro-acoustic Measurements: A Novel Approach
Eliminating the Tacho Probe
Comparison of Acoustic Holography Methods for Surface Velocity
Determination on a Vibrating Panel
 - 1 – 2005 Acoustical Solutions in the Design of a Measurement Microphone for
Surface Mounting
Combined NAH and Beamforming Using the Same Array
Patch Near-field Acoustical Holography Using a New Statistically Optimal
Method
 - 1 – 2004 Beamforming
- (Continued on cover page 3)

Technical Review

No. 1 – 2016

Contents

Flight Test Validation of Noise Models for High Performance Military Aircraft Using Beamforming.....	1
<i>Dr Ernst Grigat, Dr Jørgen Hald</i>	
Use of a Portable Flanged Impedance Tube for Absorber Design and Measurement.....	23
<i>Paul Murray</i>	

TRADEMARKS

Brüel & Kjær and all other trademarks, service marks, trade names, logos and product names are the property of Brüel & Kjær or a third-party company. Nothing in this document may be construed as granting, by implication, or otherwise any license or right to use any of the trademarks without a prior written permission of Brüel & Kjær or the owner of such trademark.

Copyright © 2010, Brüel & Kjær Sound & Vibration Measurement A/S
All rights reserved. No part of this publication may be reproduced or distributed in any form, or by any means, without prior written permission of the publishers. For details, contact:
Brüel & Kjær Sound & Vibration Measurement A/S, DK-2850 Nærum, Denmark.

Editor: Harry K. Zaveri

Flight Test Validation of Noise Models for High Performance Military Aircraft Using Beamforming

Dr Ernst Grigat¹, Dr Jørgen Hald²

Abstract

This paper gives a survey on a noise measurement flight test campaign for validation of the noise models developed within the framework of an initiative at Airbus Defence and Space GmbH to reduce the noise of high performance military aircraft. Based on a modular approach, models for the different noise sources have been developed mainly based on theoretical approaches inducing the need for according validation using noise data from flight tests. Accordingly, in a dedicated flight test campaign at Neuburg airfield in Germany, aircraft noise data were gathered supported by Brüel & Kjær which then provided validation information on noise emission and directivity characteristics for the different noise sources modelled. The system used for this was a flyover beamforming system with 135 microphones deployed on the ground.

Résumé

La présente communication rapporte les résultats d'une campagne d'essais acoustiques en vol visant à la validation de modèles développés par Airbus Defence et Space GmbH dans le cadre d'une démarche de réduction du bruit des aéronefs hautes performances à usage militaire. Les différentes sources de bruit modélisées, obtenues sur le mode modulaire de manière essentiellement théorique, devaient être validées au moyen de mesures obtenues au cours d'essais en vol réalisés sur la base aérienne de Neubourg, en Allemagne. La collecte des données de bruit a été supportée par Brüel & Kjær, qui a ensuite produit les informations relatives à la validation des différents modèles (niveaux et caractéristiques de directivité des émissions sonores). Les données d'essai ont été recueillies lors du

1 Airbus Defence and Space GmbH, Manching, Germany, ernst.grigat@airbus.com

2 Brüel & Kjær Sound & Vibration Measurement A/S, Nærum, Denmark, Jorgen.Hald@bksv.com

survol des aéronefs au moyen d'un système à formation de faisceau composé de 135 microphones de mesure déployés sur le sol.

Zusammenfassung

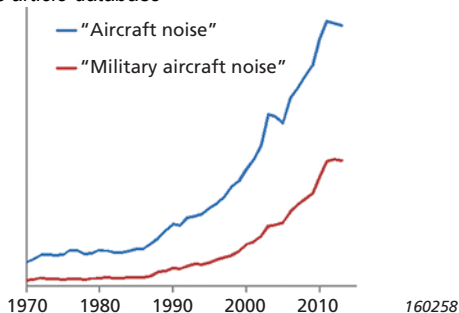
Dieser Artikel gibt einen Überblick über Lärmmessungen im Rahmen einer Flugtestkampagne zur Validierung von Geräuschmodellen, die auf Initiative der Airbus Defence and Space GmbH erfolgte, um die Geräusche von Hochleistungs-Militärflugzeugen zu reduzieren. Auf der Grundlage eines modularen Konzepts wurden Modelle für die verschiedenen Geräuschquellen entwickelt. Da die Modelle hauptsächlich auf theoretischen Ansätzen beruhen, war eine Validierung mit Lärmessdaten von Flugtests erforderlich. Zu diesem Zweck wurden in einer gezielten Flugtestkampagne mit Unterstützung von Brüel & Kjær auf dem Flugplatz Neuburg Fluglärm Daten gesammelt. Sie lieferten Validierungsdaten für die Lärmemission und Richtcharakteristik der verschiedenen modellierten Geräuschquellen. Das hierfür verwendete System war ein am Boden aufgebautes Beamforming-System für Überflugmessungen mit 135 Mikrofonen.

1. Introduction

Noise reduction for civil aircraft has been an important issue for aircraft manufacturers as well as for airport operators within the past few decades. Meanwhile, a huge set of requirements and rules coming from annoyed residents, legal regulations and customers (that is, airline companies) have to be taken into consideration.

For a long time, less emphasis has been placed on noise reduction for military aircraft due to several reasons. However, as can be seen from Fig. 1, this seems to

Fig. 1. Hits in scientific article database



be subject to change over the past years. Military aircraft noise is becoming more important as the number of hits for the respective search expressions in a scientific article database exemplarily shows.

Additionally, the respective international regulations [1] have been tightened in two steps – in 1985 and quite recently in 2006. Similar regulations exist on both European and national (for example, German) levels. Accordingly, the relevant regulations are:

- ICAO Annex 16, Volume 1, Paragraph 12.2 and 3.4.1.2a (international)
- EC Reg. 1592/2002, Articles 6 & 13 (Europe)
- LuftVZO, Article 3 (Germany)

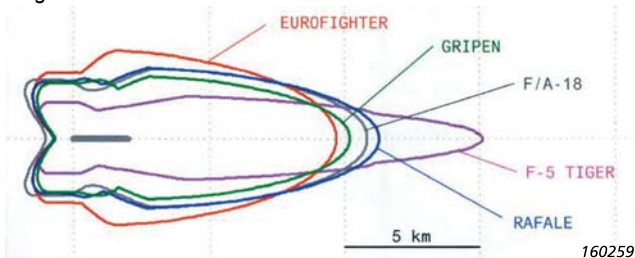
For military aircraft specifically, there is a certain shift in emphasis with respect to the relevance of noise emissions to be observed. In the past, national fighter acquisition programs usually contained no requirements with respect to noise emission/immission, whereas in the last decade, the Requests for Information or Proposal (RfI/RfP) ask for this data and information more frequently.

This is illustrated by an article [2] in the Swiss public journal, *Cockpit*, about the latest Swiss Air Force Fighter acquisition program, in which the Swiss representative ‘armasuisse,’ together with the respective aircraft manufacturers, performed flight tests that were subsequently evaluated by the Swiss institute EMPA (Fig 2).

Finally, these facts clearly lead to the necessity of developing strategies and technical solutions for (military) aircraft noise abatement.

In this paper, the overall approach and actual status of an industrial noise reduction initiative for a specific high performance military aircraft is presented. However, as the developed processes and techniques are, by their very nature, generic to a large extent, application to other aircraft (types) would be straightforward in principle.

Fig. 2. EMPA flight test noise evaluation



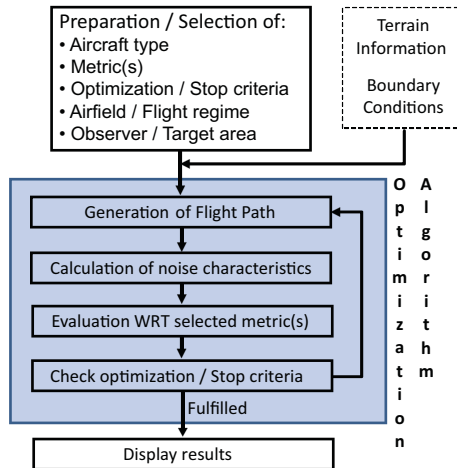
Nevertheless, as aspects of noise reduction are still of minor importance to the design and development of military aircraft, especially compared to operational requirements, the focus for the approach presented here has been mainly placed on noise immission rather than emission. Clearly, as the predominant nuisance generated by aircraft is in the vicinity of the respective airfields, the overall goal defined is the **reduction of aircraft noise ground immission by optimization of the according takeoff climb (and landing approach) flight path.**

2. Overall Approach

In pursuing the above goal, it is necessary to implement an optimization algorithm which generates noise optimal (that is, minimal) flight paths based on a dedicated set of suitable optimization criteria (noise metrics). Focus will be put on allowing a broad variety of possible flight paths and easy observance of boundary conditions (for example, flight mechanical and performance restrictions, terrain information, and residential or prohibited areas respectively), while the accuracy of the solution will be only a subordinate goal.

Therefore, from the current point of view, the use of the principles of genetic optimization (optionally including a respective niching concept for generating a set of feasible ‘optimal’ flight paths) seems to be appropriate. Developing and subsequently implementing a corresponding algorithm is, however, a very time

Fig. 3. Logic of overall approach



160260

consuming task and will therefore be accomplished towards the end of the whole program development cycle. For the time being, the definition and construction of operationally reasonable flight paths based on operational manual or flight test data, or a combination of both, should be sufficient. An overview over the main elements of the general overall approach for noise minimization can be found in Fig. 3.

The starting point, selection of aircraft, stresses the modular nature of the approach presented here. All aircraft-specific parameters (for example, engine or aerodynamics) are not hard-coded but are provided to the program by dedicated external data sets using respective generic interfaces. One crucial point for a proper setting of an optimization approach is the appropriate choice of the respective metric(s) for the evaluation of noise on ground. Accordingly, a respective comprehensive literature study has been undertaken in order to identify the most suitable metrics. In addition to a total of 14 psychoacoustic metrics, which are not taken into account at the current stage of the development, the following ‘objective’ metrics have been assessed to be suitable for comparative noise immission evaluation:

- Sound Pressure Level (A-weighted)
- Sound Exposure Level
- Equivalent Continuous Sound Level
- Time Above Specific Level
- Day-and-Night Equivalent Sound Level
- (Effective) Perceived Noise Level

In the selection of optimization/stop criteria, it is fixed for whether one single optimal solution, or rather a set of feasible flight paths fulfilling, for example, accuracy requirements, is searched. Additionally, the maximum number of iterations is set.

Furthermore, in the selection of the airfield, the local coordinate system is fixed by choosing a geographic point using World Geodetic System 1984 (GDS 84) or GPS (Navstar) coordinates to represent the airfield where the takeoff (or landing) is performed. Additionally, the position of the observer, or an appropriate area on ground, is defined for which the chosen noise metric(s) will be evaluated.

Prior to the start of the actual optimization algorithm, databases with additional information on terrain specifics and possible boundary conditions (for example, residential or restricted areas) are fed into the program via their respective modular interfaces.

The first step within the optimization algorithm will be the selection or generation of a dedicated flight path that is a candidate for the optimum solution to be found. After the calculation of the noise characteristics along the flight path, the above chosen on-ground noise metrics have to be evaluated, thus providing a basis for the subsequent decision on continuation of the optimization iteration. In case the optimization process is continued, a new ‘candidate’ flight path has to be constructed based on previous results (feedback loop). The methods and principles which are applied for this purpose constitute the very core of an optimization approach/algorithm.

If the stop criterion is fulfilled, the results will be displayed using a dedicated user interface. Furthermore, all relevant and necessary data for potential post processing (for example, detailed analysis of feasible flight paths) are stored in accordingly designed databases.

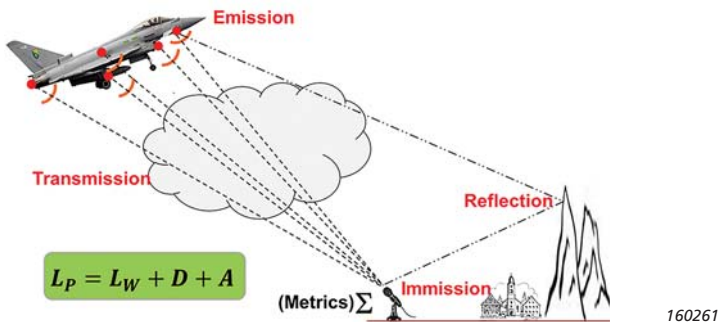
3. Noise Calculation Model

As a basis for the above mentioned optimization approach, a dedicated validated aircraft noise calculation model has to be provided. Accordingly, a dedicated generic modular approach has been developed.

As it can be seen in Fig. 4, this approach mainly consists of a combination of three main components:

- Emission (analytic modular approach)
- Transmission (modified/simplified ray tracing)
- Immission (metrics and refraction)

Fig. 4. Modular aircraft noise model



This is also formally reflected in the common equation for aircraft noise propagation according to [3],

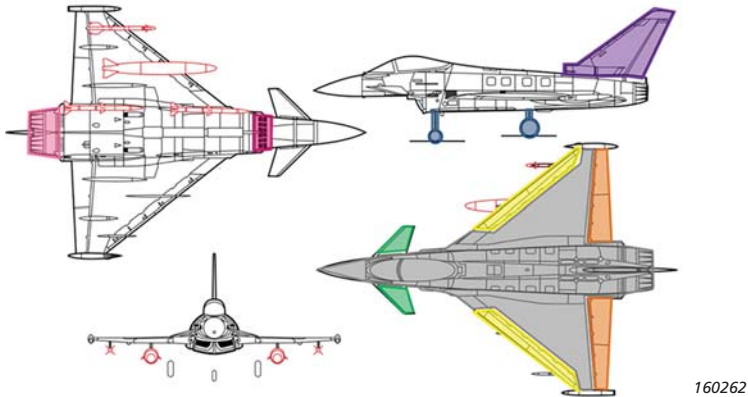
$$L_p = L_W + D + A \quad (1)$$

where L_p denotes the sound pressure level, L_W the sound power level, D the directivity correction, and A the absorption during propagation. The above breakdown, which is defined analogously to [4], has the advantage that the three components can be encapsulated to a large extent, which eases development of the three models independently from each other. This process and the respective current status will be described in more detail in the following subsections.

3.1 Noise Emission (Aircraft Noise)

The basic principles and current status of the noise emission model used for the approach described in this paper are outlined in detail in [5, 6 and 7], and an overview is given in this section.

Fig. 5. Aircraft noise emission components



As depicted in Fig. 5, the basic approach consists of splitting up the overall noise source ‘aircraft’ into the following distinct noise source components:

- Engine jet (including combustion and after burner)
- Engine fan (broadband and discrete tone)
- Undercarriage (nose and main landing gear)
- Vertical tail

- Foreplane
- Leading and trailing edge
- Airframe
- Stores

For each of these noise sources, a dedicated noise emission model, as well as a respective directivity correction, has to be provided. As shown in a subsequent section, the noise propagation is modelled separately for each source. Therefore, the combination of the noise components is not performed until impact at the observer position.

Initially, engine and airframe noise are modelled using primarily analytical formulas (provided in [4]) and will be subject to corrections based on the results of validation flight test measurements.

Having modelled the individual noise emission of each engine source, the second component of the complete emission model consists of the near-field behaviour of the noise, that is, the directivity corrections for all sources.

It is well known that fan and jet noise emissions, at least vertically, do not show a homogenous expansion. Analogously, a similar phenomenon is also expected horizontally, especially in the case of a twin engine aircraft with two parallel engines mutually influencing the exhaust airflow. It is therefore essential to consider a three-dimensional directivity correction.

However, no straightforward analytical approach exists for the synthesis of these corrections, which induces the need for initially modelling respective directivity functions partly based on heuristics and existing tests (that is, noise measurements) for other aircraft.

For all other components (except the leading edge), noise emission is basically modelled by some equation of the form:

$$P_{component} = C_{component} \cdot \bar{q} \cdot Ma \cdot \frac{\sqrt{A}}{r_{ref}} \cdot F(V) \quad (2)$$

where C is a component specific constant, \bar{q} the dynamic pressure, Ma the Mach number, A and r_{ref} reference area and length, and $F(V)$ a function based on airspeed number. With respect to directivity, all these noise emission components are assumed to be approximately monopoles, therefore no directivity correction has to be applied.

3.2 Noise Transmission (Propagation)

Having modelled the noise emitted in the near field of the aircraft, the proximate task consists of specifying the propagation to (an observer on) the ground. As described in [8], a simplified (linearized) ray-tracing method has been established to be of sufficient accuracy in this case and subsequently implemented. Initially based on the principles of geometric acoustics, the method developed here mainly introduces the aspect of the time dependency to noise propagation.

A general characteristic of noise (or more generally sound) propagation through the atmosphere is the phenomenon of attenuation (or absorption), also contained in Eq. 1. Usually the following three different types of absorption are distinguished:

- **Geometric:** radially expanding, the sound power is distributed over an area increasing with distance from the source and, therefore, the sound power per area unit decreases proportionally to the square of the distance
- **Atmospheric:** reduction of sound intensity due to molecular air absorption
- **Ground:** additional sound attenuation for observer location with an aircraft ground angle lower than 15° , mainly applicable for airfield operation or very low flight altitudes

Transmission phase ends with sound impact at the observer as described in the following subsection.

3.3 Noise Immission (Observer Perception)

As shown in Eq. 1, the characterization and measurement of the noise perceived by an observer on the ground, the so-called sound pressure level L_P is crucial in contrast to the sound power level L_W which describes the noise emitted by the aircraft. Accordingly, the most important effects that impact noise on the ground are:

- **Ground absorption** (as described in the preceding subsection)
- **Reflection:** of utmost importance, especially in the case of the airfield and observer being in the vicinity of mountains, as in Switzerland, or in an area with many buildings
- **Bending:** deflection due to obstacles

To begin with, the latter two effects are currently not modelled but will be taken into account in future program versions. Furthermore, the current model of the ground as planar surface will then be replaced by a proper ground model based on a terrain database. Refined modelling, up to a level of detail containing buildings, is currently not planned.

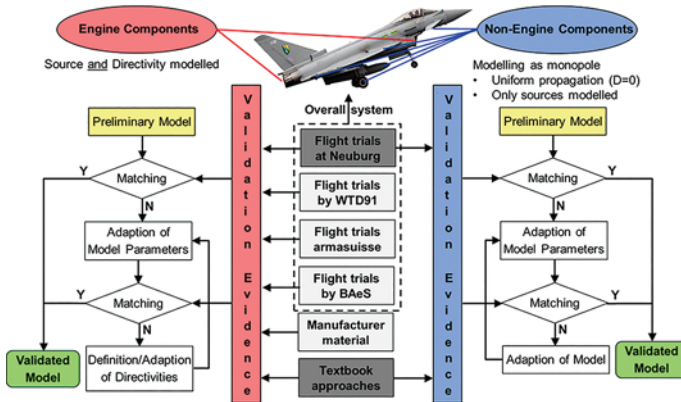
4. Validation Approach

As already indicated with respect to modelling, distinct approaches for engine and non-engine noise emission components have been chosen, and this strategy has been pursued for validation. Despite this distinction, all models share the fact that they are originally based on textbook formulas. Moreover, the dedicated validation flight tests described below are also aiming at substantiation or refinement (where applicable) of all noise emission models. There is some additional information from tests performed in the past that can be used selectively for noise model validation purposes, however due to the respective measurement approaches, application is limited to engine noise.

Generally, engine (fan, combustion, jet) noise validation is performed in a first step by comparing noise emission data calculated/derived from measured noise data with the data provided by the corresponding emission model for the respective test conditions. Subsequently, matching of the respective data sets/curves is attempted by fine-tuning suitable model parameters. In the case that, after this refinement process, there are still some significant discrepancies, it is assumed that these are due to the respective directivity characteristics. The discrepancies therefore, are allotted to these characteristics which, at least for the engine, are not modelled analytically but have to be derived from heuristic approaches refined by noise measurement test data as described above.

For non-engine noise emission models, the first validation step consists, as above, of the comparison of noise emission data calculated/derived from measured noise data with the data provided by the corresponding emission model for the

Fig. 6. Noise model validation approach



160263

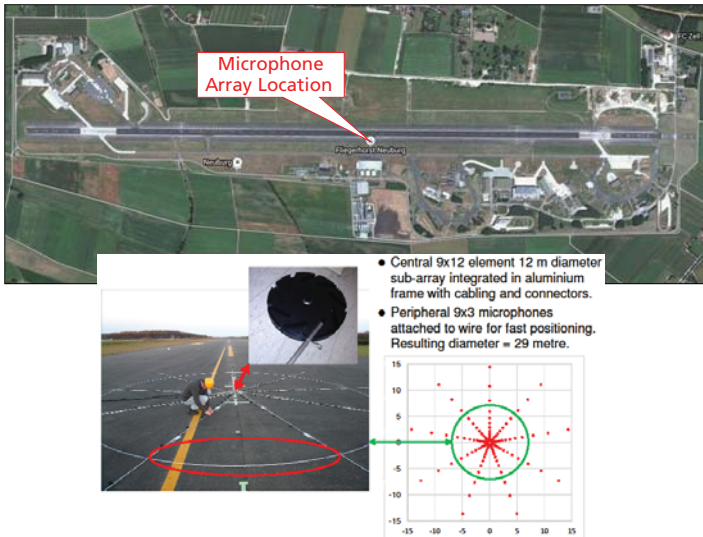
respective test conditions. However, in this case, potential remaining discrepancies after matching test and model data cannot be attributed to directivity characteristics as the non-engine noise emission models are assumed to be monopoles as described earlier. Therefore, in order to achieve a proper match of data/curves for validation, the model itself has to be adapted accordingly. The complete process is presented in Fig. 6.

The tests performed by WTD91, armasuisse and BAeS, as well as additional engine manufacturer material are exclusively used as additional information for engine noise model validation.

5. Noise Model Validation Flight Tests

As described above, for substantiation, refinement, and validation of the noise emission models originally developed on a mainly analytical/textbook basis, respective noise measurement flight tests are essential. Accordingly, in a two-day campaign, appropriate flight tests have been performed in November 2015 at Neuburg airfield (Fig. 7), with the support of the Danish company Brüel & Kjær which provided the noise measurement equipment (135 microphone array, recording hardware, etc.) and conducted the noise recording and post-processing.

Fig. 7. Noise measurement setup at Neuburg



160264

A total of 20 test points (flyovers) have been performed in different configurations (with and without under wing tanks, undercarriage up and down) and with varying power settings (part dry, maximum dry, maximum afterburner) at altitudes between 150 and 200 ft (45 and 60 m) above the airfield.

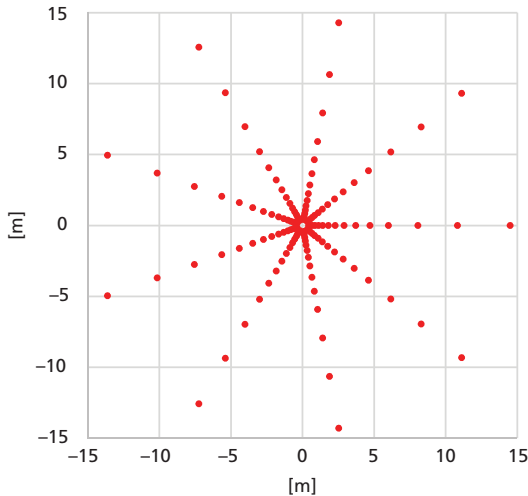
Subsequent to this flight test campaign, the recorded noise data have been analysed, evaluated, and processed by Brüel & Kjær [9] for the validation purposes as described in the following section.

6. Description of the Beamforming System

The principles implemented in the applied system are described in references [10 and 11]. Actually, the applied array design, shown in Fig. 8, is identical with that described in [11], having 135 microphones within a diameter of 29 m.

Air turbulence will introduce random phase modulation of the recorded pressure signals, the modulation being identical for two microphones close to each other, but incoherent for widely separated microphones. As a result, coherence will be lost between widely separated microphones, even for signal components from the same source. The radius within which coherence is retained turns out to typically be $4000 \text{ Hz} \times \text{meter/Frequency}$, which is 1 m at 4 kHz. Due to this, only a central part of the array is active at each frequency, the radius of the active part being

Fig. 8. The applied array geometry consisting of nine identical line arrays. Each array contains 15 microphones with exponentially increasing distances to the centre



160265

inversely proportional to frequency. At high frequencies, only the very central part is used, requiring small microphone spacing, while the peripheral array sections are active only at the lowest frequencies, allowing the use of a large microphone spacing.

Due to the limited spatial coherence, the angular resolution will be limited to around 3° over a wide frequency range, corresponding to 2.5 m resolution on an aircraft at an altitude of 50 m above the array. This resolution is achieved only with the aircraft close to the vertical array axis. Beyond 30° from the array axis, the resolution quickly vanishes.

Each measurement consists of simultaneous recording of the sound pressure time signals from the 135 array microphones distributed on rigid surfaces on the ground. Some microphones were on a concrete surface, while the remaining ones were placed on wooden plates. The horizontal xy -coordinates were defined by the array structure, while all vertical positions were measured. In order to focus on a selected point on the moving aircraft, the position of that point relative to the array must be known for each sample in the recording of the microphone signals. Since the flight track is recorded in the aircraft, while the microphone signals are recorded on the ground, GPS time stamps were recorded both with the flight track data in the aircraft and with the array data on the ground to support a subsequent alignment in time.

7. Beamforming Processing

The applied beamforming system performs a two-step calculation:

- 1) Tracking time domain Delay and Sum (DAS) beamforming, followed by FFT (Fast Fourier Transformation) and averaging in time intervals during which the aircraft moved 10 m. The averaging time was typically 0.1 s.
- 2) Deconvolution, where the amplitude distribution is estimated for a source model that consists of a mesh of incoherent monopole point sources in the mapping plane near the underside of the aircraft. The amplitude distribution is estimated in such a way that a measurement on the source model would generate a DAS map as close as possible to the one obtained in the first step. The source model well represents the sound radiation towards the array, even for sources that are not omnidirectional. Based on measurements with the array at different angles from the aircraft, the sound power of aircraft components and the related directivity characteristics can be estimated.

The tracking DAS beamforming system automatically performs Doppler frequency correction, meaning that the estimated spectra will represent the frequencies on the aircraft. When calculating sound power data (or sound intensity) on the aircraft, correction is also performed for the following:

- Doppler amplitude effects
- Spherical spreading
- Atmospheric loss during sound propagation from the aircraft to the array
- Doubling of the sound pressure at the microphones due to the rigid ground surface

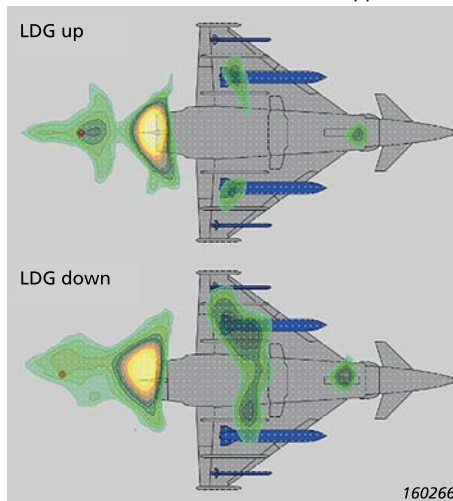
8. Results from Beamforming

8.1 Level Flight at 200 kt

This rather low engine power setting allows the identification of secondary noise sources on the aircraft.

Fig. 9 contains sound intensity maps from two comparable flyovers with landing gear up and down, respectively. Both flyovers were with external tanks on the aircraft, with a constant speed of 200 kt (approx. 100 m/s) and at an altitude

Fig. 9. Comparable sound intensity maps with landing gear up and down, respectively. Display range is 20 dB, and the same threshold has been applied in both plots



around 47 m above the array. Averaging was performed over 10 m intervals, 20 m before the aircraft reached the vertical array axis, and the plots represent the frequency range from 192 to 4992 Hz with linear weighting.

Based on maps like those in Fig. 9, component sound power spectra can be estimated by integration over associated areas in the maps. However, such spectra will assume omnidirectional radiation from all points in the maps because a source model of monopole point sources has been used. By combining maps from different positions of the aircraft during a flyover above the array, information about the directivity in a vertical plane can be obtained within a certain angular range. When the aircraft is more than 45° away from the vertical array axis, the resolution on the mapping plane vanishes. Valid directivity information for noise source components (intake, jet, etc.) on the aircraft can therefore typically be obtained only between 45° and 135° from the aircraft forward direction. Outside that range, some reasonable approximation must be used. At angles smaller than 45° (close to forward), the directivity has been assumed to remain constant and equal to the value at 45° . A corresponding assumption has been used for angles larger than 135° . For the jet and intake sources, it is reasonable to assume the noise radiation towards the lower hemisphere to be rotational symmetric around the longitudinal axis of the aircraft. Under that assumption, the sound power and the directivity of these two sources can be estimated based on a single flyover.

Fig. 10 contains estimated sound power spectra for the full aircraft and for five components: jet, intake, centre (mainly the landing gear), external tanks and the sections of the wings outside the tanks. For all these sources we have assumed the noise radiation into the lower hemisphere to be rotationally symmetric around the

Fig. 10. Estimated sound power spectra from a single flyover with a constant speed of 200 kt, external tanks and landing gear (LDG) down

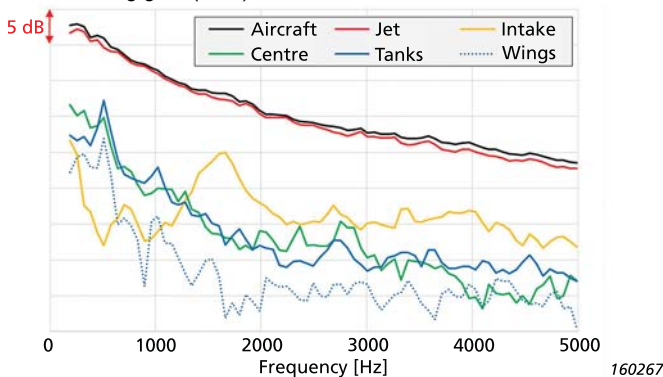
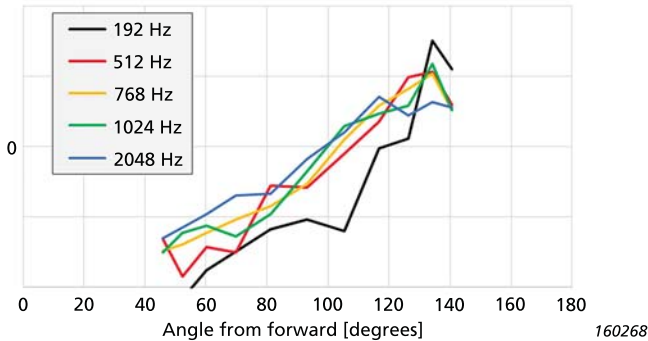


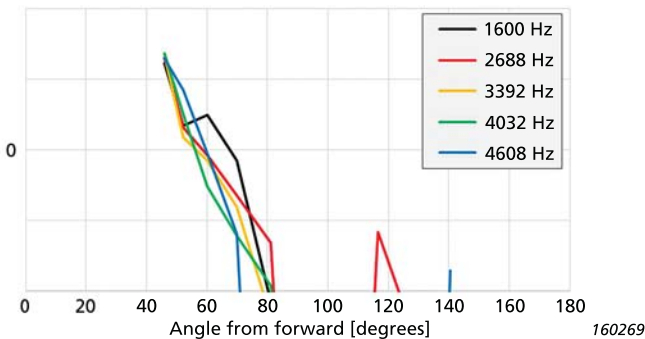
Fig. 11. Estimated directivity patterns of the jet noise at five selected frequencies for the flyover represented in Fig. 10



aircraft's longitudinal axis. The spectra are from the same measurement as the lower map in Fig. 9, that is, 200 kt with landing gear down, and the aircraft position interval is also the same. Clearly, the jet is the dominating source over the full frequency range. Above 1.2 kHz, the intake has a significant contribution with a peak around 1.6 kHz. As can be seen in the lower map of Fig. 9, the contributions from the tanks and from the rear wheels of the landing gear do not have good resolution. The related spectral peak at 500 Hz in Fig. 10 can therefore represent noise from either of the two sources.

Fig. 11 and Fig. 12 contain directivity patterns at selected frequencies for the jet and for the engine intake respectively, based on the same measurement as represented in Fig. 10, that is, 200 kt and landing gear down. For the jet, a wide range of frequencies has been chosen with a focus in the low end of the spectrum,

Fig. 12. Estimated directivity patterns of the intake noise at five selected frequencies for the flyover represented in Fig. 10



where most of the radiated power is concentrated. For the intake, a set of frequencies have been chosen where there are spectral peaks above 1.2 kHz. Only the angular range with beamforming data is covered, that is, typically between 45° and 135°. As expected, the jet noise radiates mostly backwards, covering a rather wide angular range. The intake noise has a very strong forward directivity.

8.2 Maximum Reheat Power Setting

With maximum reheat (afterburner) engine power setting, the jet noise is so strong that all other sources will be outside of the dynamic range provided by the array: the ghost sources due to the jet will mask all the other low-level sources.

Fig. 13 contains sound intensity maps from a flyover with landing gear up and without the two external tanks. The speed was 154 m/s when the aircraft passed vertically over the array at an altitude of 47 m. Again, averaging is performed over 10 m intervals, 20 m before the aircraft reached the vertical array axis, and the plot represents the frequency range from 192 to 4992 Hz with linear weighting.

The series of ghost sources along a line from the jet to the top right corner are due to a combination of strong Doppler shifts (Mach 0.45) and side lobes of the array. For each real source, the side lobes will introduce a set of ghost sources at lower levels. Without Doppler shifts, ghost sources due to a specific real source will appear only in the same frequency band as the source itself. In that case, deconvolution is effective at suppressing side lobes. However, with Doppler shifts, some of the ghost sources may appear in different frequency bands than the real source. Since deconvolution is operating with data in a single frequency band, it cannot suppress these ghost sources. Clearly, the Doppler-shift jet related ghost sources in Fig. 13 are at higher levels than all other real sources, which cannot therefore be identified and quantified.

Fig. 13. Overall sound intensity map from a flyover with maximum reheat power setting. Display range is 20 dB.

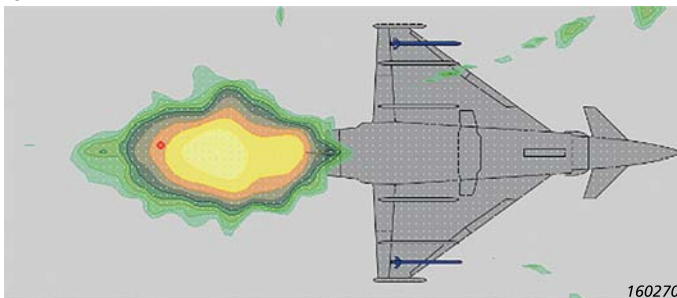


Fig. 14. Estimated sound power spectra from a single flyover with maximum reheat power setting, external tanks off and landing gear (LDG) up

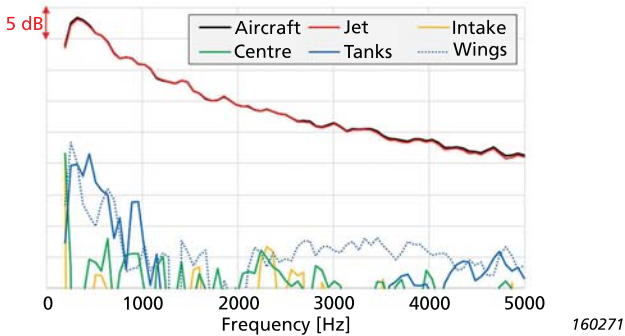
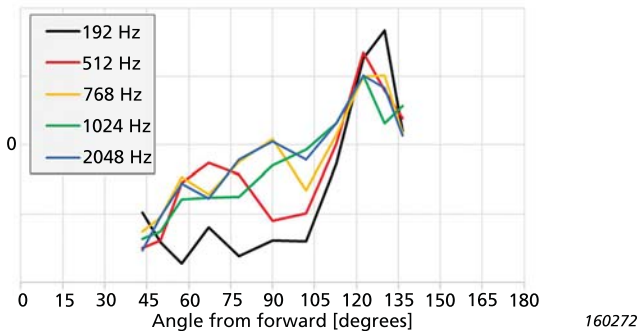


Fig. 14 contains maximum reheat sound power spectra for the same components/areas as represented in Fig. 10, with the areas of the tanks being retained although no tanks are fitted. The aircraft position interval is also the same, that is, 20 m before the aircraft passes over the array axis. Clearly, the jet is the dominating source over the full frequency range. The spectra of the remaining areas are due to ghost sources, the main contributions being in the areas named tanks and wings, which contain Doppler-shift ghost sources due to the jet as described above.

Fig. 15 shows the directivity pattern of the jet noise at a set of frequencies. Compared with the corresponding curves in Fig. 11 (200 kt constant speed), the directivity characteristics are similar at 192 Hz. Particularly, 512 Hz shows a sharper directivity of the maximum reheat radiation than the radiation at 200 kt constant speed.

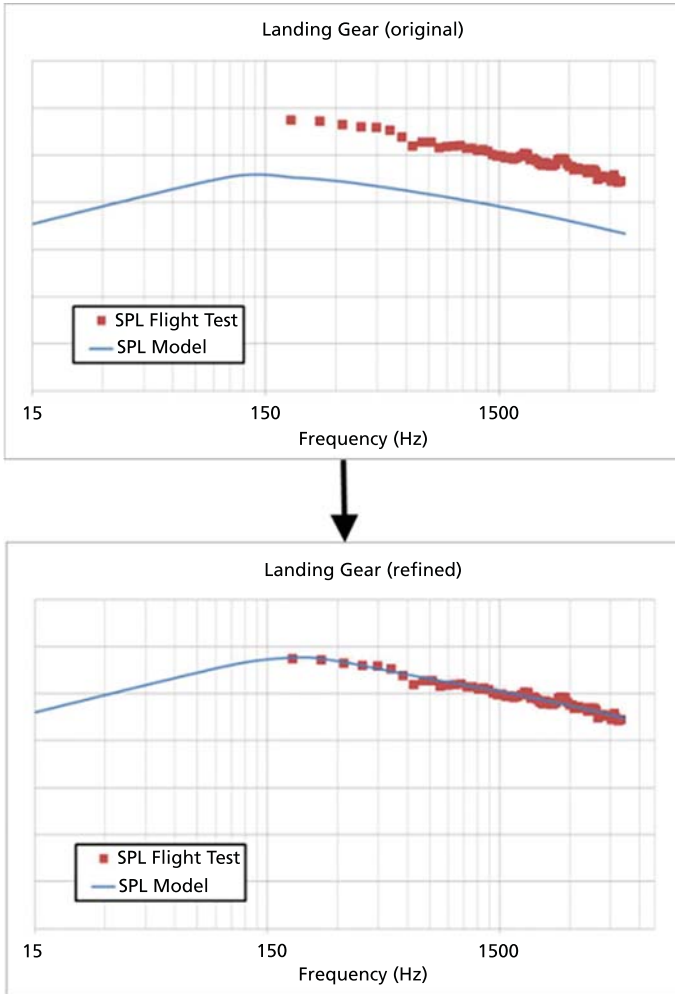
Fig. 15. Estimated directivity patterns of the jet noise at five selected frequencies for the flyover represented in Fig. 13 and Fig. 14



9. Model Refinement and Update

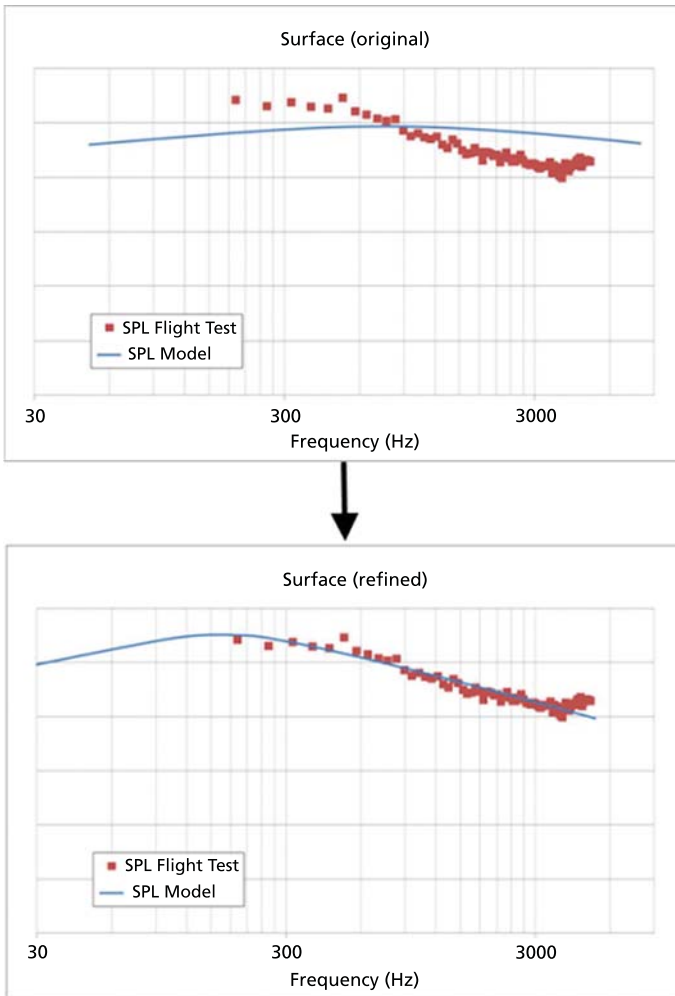
Using the noise emission data based on flight test measurements and synthesized by the beamforming technique described above, the existing analytical noise source models can be refined and updated, and therefore validated.

Fig. 16. Undercarriage noise model refinement



160273

Fig. 17. Airframe noise model refinement



Representing the current status and progress of the ongoing refinement and validation activities, the first results presented in the previous figures focus on the treatment of the non-engine noise source components (as described in the general validation strategy, Fig. 6) which are characterized by a uniform omnidirectional sound propagation (monopole modelling).

According to the approach described in “Validation Approach” (Section 4), the results for the sound power characteristics for each noise source obtained by the beamforming process, described in the preceding sections, is compared to the actual (analytical) model, thus leading to respective corrections and/or refinements of the model.

Accordingly, either model parameters have been adjusted, for example, for the landing gear (Fig. 16), or the complete model (function) has to be corrected, for example, for the airframe (Fig. 17.)

Differences have been evaluated over a carefully chosen frequency spectrum with special consideration of the feasibility of the noise measurement results, also taking into account the relevance of the respective frequency band.

In both cases, a very good match of flight test and model data could be obtained, and therefore, at least these two source models can be looked upon as being validated. For a complete validation of the noise calculation model, however, all noise emission (source) models have to be validated as well as the noise propagation (transmission) algorithm.

10. Summary and Conclusions

A generic approach for noise modelling of high performance military aircraft substantiated by a corresponding validation flight test campaign has been presented. Due to the modular structure of the aircraft noise model, each noise source can be modelled and validated separately thus giving way to flexibility for a wide variety of applications.

A dedicated validation strategy for this approach has been developed and an according flight test campaign and evaluation phase using the beamforming technique has been performed, leading to initially promising results. Thus both, the noise source modelling approach, as well as application of beamforming have been proved to be feasible approaches.

Future planned activities with respect to enhancement of the described aircraft noise calculation program include the completion of the validation process including the algorithms for noise propagation / transmission, the integration of a feasible terrain database, the development of a comfortable graphical user interface, and finally the embedding of the noise calculation model into a flight path optimization algorithm.

11. References

- [1] ICAO International Standards and Recommended Practices, Annex 16 to the Convention on International Civil Aviation – Environmental Protection, Volume 1, Aircraft Noise, Sixth Edition, July 2011.
- [2] Hodel, W. (2010). Viel Lärm um nichts?, in *Cockpit – das SchweizerLuftfahrt-Magazin*, Nr.1.
- [3] ISO 9613: Acoustics – Attenuation of Sound During Propagation Outdoors – Part 2: General Method of Calculation, 1996.
- [4] Filippone, A.(2012). *Advanced Aircraft Flight Performance*, Cambridge University Press.
- [5] Mayer, S.(2014). *Modellierung von Schalleistungspegeln an Kampfflugzeugen*, Bachelor Thesis, TH Ingolstadt.
- [6] Walter, M. (2015). *Erweiterung eines 2D Emissionsmodells für Fluglärm auf die Berücksichtigung von Höheninformation*, Bachelor Thesis, TH Ingolstadt.
- [7] Walter, J. (2015). *Umströmungsgeräusche: Auswahl und Beschreibung der Lärmquellen eines Hochleistungsflugzeuges*, Internship Report, TH Ingolstadt.
- [8] Peterlik, T. (2015). *Implementierung eines vereinfachten Ray-Tracing Verfahrens zur Schallausbreitung in ein bestehendes Softwaremodell*, Bachelor Thesis, TH Ingolstadt.
- [9] Hald, J. (2016). Fly-Over Beamforming on Eurofighter Typhoon, Brüel&Kjær.
- [10] Hald, J., Ishii, Y., Ishii, T., Oinuma, H., Nagai, K., Yokoyama, Y., and Yamamoto, K. (2012). High-resolution fly-over Beamforming using a small practical array, AIAA Paper 2012-2229.
- [11] Ishii, Y., Hald, J., Ishii, T., Oinuma, H., Nagai, K., Yokoyama, Y., and Yamamoto, K. (2016). High-resolution fly-over Beamforming using a practical array, Berlin Beamforming Conference 2016, Paper BeBec-2014-16.

Use of a Portable Flanged Impedance Tube for Absorber Design and Measurement

*Paul Murray*¹

Abstract

Acoustic material testing is becoming increasingly relevant to engineers, designers and manufacturers from a broad range of industries. This paper presents comparisons between material absorption measurements made using the traditional approaches of the reverberation room method and the fixed impedance tube using a sample holder, with those obtained using a lightweight portable flanged impedance tube method.

The portable tube allows fast non-destructive in situ material measurements. It may therefore be used to measure the impact of the installation (for example, effects of facing sheets, curvature, material compression, bagging, etc.)

Results are presented for both non-locally reacting and locally reacting materials. The portable tube results are compared directly with in-tube data. They are also corrected for random incidence to allow comparison with the diffuse field reverberation room data. It is concluded that the flanged portable impedance tube method provides an attractive alternative to existing methods.

Résumé

Dans de nombreux secteurs de l'industrie, les essais de caractérisation des matériaux acoustiques deviennent une étape incontournable pour les fabricants, concepteurs et ingénieurs de bureaux d'études. La présente communication compare aux mesures d'absorption réalisées au moyen de la méthode traditionnelle, avec tube d'impédance fixe à porte échantillon en chambre reverberante, les mesures obtenues avec un tube d'impédance à collerette, portatif et léger.

Le tube portatif permet de réaliser rapidement, sur le terrain, des mesures non destructives sur les matériaux. Il peut donc être utilisé pour caractériser l'ensemble

¹ Acoustic Consultant, Morrisbrand Ltd, Horsham, W. Sussex, UK, paulbmurray@morrisbrand.co.uk

d'une installation (plaques se faisant face, courbure, compression de matériaux, emballage, etc..)

Les résultats présentés ici concernent les matériaux localement réactifs et non localement réactifs. Les mesures obtenues avec le tube portatif sont directement comparées avec les données à l'intérieur du tube. Avec aussi une correction d'incidence aléatoire pour permettre la comparaison avec les données champ diffus de la chambre réverbérante. Il est avancé en conclusion que la méthode avec tube d'impédance portatif constitue une alternative intéressante aux méthodes existantes.

Zusammenfassung

Akustische Materialprüfungen gewinnen zunehmend an Bedeutung für Ingenieure, Designer und Hersteller in zahlreichen Branchen. In diesem Artikel werden Messungen der Materialabsorption miteinander verglichen und übliche Hallraumverfahren mit festem Impedanzrohr und Probenhalter einem Verfahren gegenübergestellt, das ein leichtes, transportables Impedanzrohr mit Flansch verwendet.

Das tragbare Rohr ermöglicht schnelle, zerstörungsfreie In-situ-Messungen an Materialien. Es ist deshalb geeignet, den Einfluss der Installation zu ermitteln (zum Beispiel die Auswirkung von einander zugewandten Platten, Krümmungen, Materialverdichtung, Ausbuchtungen etc.)

Es werden Ergebnisse sowohl für nicht-lokal reagierende als auch für lokal reagierende Materialien präsentiert. Mit dem tragbaren Rohr und im festen Rohr gemessene Daten werden direkt miteinander verglichen. Es erfolgt auch eine Korrektur, um den Vergleich mit den Hallraumdaten im diffusen Schallfeld zu ermöglichen. Die Schlussfolgerung lautet, dass das tragbare Rohr mit Flansch eine attraktive Alternative zu den bisherigen Verfahren darstellt.

Introduction

Acoustic material absorption may be measured using a number of approaches. These include the diffuse field reverberation room method [1, 2] the Kundt tube with sample holder method [3, 4, 5], the Adrienne in situ reflection method [6], and the Microflown PU probe method [7]. This paper reports on the use of an alternative non-destructive method, which is currently used for impedance measurement of aero engine acoustic panels. The method involves adding a flange to a Kundt tube, allowing it to be used non-destructively for in situ measurements.

This work has been prompted largely by an identified need for in situ measurements of materials in their final installed state, which are not always representative of laboratory installations. Reference [8] reports on two variants in the signal processing of the reflection method. These provide similar results for materials of high absorption coefficient, but are less accurate at low frequencies, with the uncertainty driven by the geometry of the measurement space. Reference [9] compares the reflection method with the reverberation room method and also with the Kundt tube sample holder method. The authors point out the errors introduced in the sample holder method when the samples are not perfectly cut to the inner diameter. However, they also report on general agreement between the sample holder method and the reverberation room method. It is noted that the reflection method provides significantly lower absorption values at mid-range frequencies (~500 Hz to 4 kHz), and generally agrees with the other two methods at higher frequencies. The authors point to limitations of the reflection method for the small sample sizes used.

Reference [10] compares the reverberation room method and the sample holder Kundt tube method with three different manifestations of the PU probe (mirror source method, plane wave surface impedance method, and intensity method). The PU probe was used to measure samples in rooms with varying levels of reverberation and size, for the mirror source and plane wave impedance methods. The results show relatively little impact of the test room environment. Subsequent comparisons were made of all three PU methods with the reverberation room and the Kundt tube sample holder methods. All methods show fairly good agreement for high frequencies (above between 1 kHz and 2.5 kHz respectively, depending on the material type), while they begin to diverge at lower frequencies. The Kundt tube sample holder method agrees best with the PU measurements at lower frequencies. However, the reverberation room method measured consistently higher levels of absorption below either 1 or 2 kHz, depending on the sample type. It is also noted that the plane wave impedance PU method was performed with a sound source at normal incidence and with a diffuse field, showing this method to be independent of the field type.

The reflection method and the Microflown PU methods have been proposed for in situ measurement of absorption coefficient spectra. A significant benefit of the flanged Kundt tube in situ method over the Microflown is that it also provides the acoustic impedance, in addition to the absorption coefficient. Flanged tube measurements are made using a well-defined source and source-to-sample distance. As opposed to the measurement of absorption only, which provides a

peak level and a variation with frequency, the measurement also of impedance permits an assessment of the frequency-dependent resistive and reactive components of a given installation, which may then be re-tuned (if necessary) to provide improved absorption per unit area.

In addition to providing in situ capability, this paper also identifies the benefits of a portable flanged impedance tube as an alternative or complement to the reverberation room and Kundt tube with sample holder methods. Work from previous authors has highlighted the relatively high levels of uncertainty in reverberation room measurements [11, 12, 13, 14, 15] and the difficulties of dealing with the effect of edge diffraction, along with the difficulties in preparing samples for sample holder Kundt tube measurements.

The test materials reported in this study included a locally reacting single layer perforate panel with honeycomb core, and a non-locally reacting acoustic tile with a high density glass wool core. Tests were performed using the reverberation room method (absorption only), the Kundt tube sample holder method, and the flanged portable impedance (Kundt) tube method.

In order to compare the impedance tube results with the reverberation room data, the flanged impedance tube results were corrected for random incidence to simulate diffuse field conditions. This was done using Fahy's method [16]. Although the high density glass wool acoustic tile was not strictly locally reacting, both sets of impedance and absorption coefficient results were corrected using this approach.

The body of this paper begins with a description of the three measurement methods used in the reported testing, and a description of the test samples. This is followed with presentation and analysis of the results. Conclusions are then drawn from the study, with recommendations made for future investigations. Finally, the contributors to this work are acknowledged.

Methods

Reverberation Decay Time Method

The procedure for measurement of panel absorption using the reverberation room method is outlined in ASTM C423-09a [1] and ISO 354 [2]. The ISO standard specifies target conditions for the test room in terms of volume, shape, absorption, diffusivity, and the sample size and installation. The number of recommended source and microphone locations is also specified, along with limits on the

ambient test conditions (temperature, humidity). Two source procedures are defined: interrupted noise and impulse response methods.

The interrupted source method is used for the tests reported here, averaged over 12 measurements (three omnidirectional source locations and four microphone locations). The reverberation time, T_{20} , was calculated for each test configuration using the part of the decay curves between 5 dB and 25 dB below the source level, with ten averages made per source/microphone location. Measurements were made at 1/3-octave frequencies between 100 Hz and 5 kHz.

The average reverberation time was measured with and without the test panel installed in the room. From these reverberation times, the equivalent sound absorption area of the test specimen, A_T , and the sound absorption coefficient, α_s , for the sample materials was calculated for each 1/3-octave frequency using Sabine's equation,

$$\alpha_s = \frac{A_T}{S} = \frac{(A_2 - A_1)}{S} = \frac{55.3V}{S} \left\{ \frac{1}{c_2 T_2} - \frac{1}{c_1 T_1} \right\} - 4V \{m_2 - m_1\} \quad (1)$$

where V is the room volume (m^3), S is the total panel area (m^2), c is the speed of sound (m/s), T_1 is the hard wall, and T_2 is the lined, reverberation time (s), and m is the power attenuation coefficient, defined as $m = \text{Atten}/10\log(e)$ where Atten (dB/m) is the atmospheric attenuation coefficient for the ambient room conditions. The room temperature and humidity varied negligibly for the tests performed.

The Brüel & Kjær test room (Fig. 1), in Nærum, Denmark, was used for the tests. It has non-parallel walls, with one vertical wall and the ceiling serrated. The

Fig. 1. Brüel & Kjær reverberation room, Nærum, Denmark



room volume is 209.6 m³. The ceiling is a little low and the maximum diagonal length is 12.4 m, which exceeds the ISO target of 11.3 m (1.9V^{1/3}) and points to potentially non-ideal diffuse field conditions. The measured standard deviations were in good agreement with those specified in Reference [1], above 400 Hz.

Impedance Tube Method

The impedance tube, or Kundt tube, method is specified in ASTM E1050-12 [3] and ISO 10534-2 [4]. A sound source is applied at one end of a cylindrical, thick-walled tube. When the opposite end of the tube is placed on a test sample, a standing wave is created. Two flush-mounted and phase-matched wall microphones are located on the tube wall. When a broadband source is used, the transfer function, H , between the microphones is used to extract the sample reflection coefficient spectrum and subsequently also the absorption and the impedance spectra. The inner diameter of the tube is chosen to ensure only a plane wave propagates in the frequency range of interest, while the microphone spacing is chosen for maximum accuracy in the desired frequency range.

The normal incidence complex reflection factor, R , is given by

$$R = |R|e^{j\phi} = R_r + R_i = \left\{ \frac{H - e^{-jks}}{e^{jks} - H} \right\} e^{2jks} \quad (2)$$

where s is the distance between the wall microphones, and x_I is the distance from the sample surface to the furthest microphone.

The normal incidence absorption coefficient, α , and normal incidence specific acoustic impedance ratio, Z , are given respectively by

$$\alpha = 1 - |R|^2 \quad (3)$$

$$Z = \frac{1 + R}{1 - R} \quad (4)$$

The normal incidence impedance ratio, Z , is the complex ratio between the acoustic pressure and particle velocity at the sample surface. It therefore generally has a real (r) and imaginary component (x), $Z = r + jx$, where r is the acoustic resistance and x is the acoustic reactance.

Fig. 2. Brüel & Kjær Portable Impedance System Type 9737



It is noted that the absorption coefficient is determined from $|R|$, which is a function only of the transfer function, H , and the distance between the two microphones, s .

It is independent of the distance from the sample surface to the microphones, x_I . If the impedance is to be extracted accurately, the distance to the sample surface must also be known to a high degree of accuracy (within 0.2 mm). A hard wall calibration routine is performed to calculate this distance.

The 29 mm inner diameter Brüel & Kjær portable flanged impedance tube (Type WA-1599-W-005) used here is shown in Fig. 2, along with the rest of the Type 9737 system. The tube diameter and microphone spacing allow the meter to be used between 500 and 6400 Hz. It also has a sample holder (Fig. 2) which accommodates materials up to a depth of approximately 200 mm. The speaker permits testing at levels exceeding 150 dB, which may be used to measure the non-linear response of a material. The tests in this report were performed at 120 dB OASPL (overall sound pressure level), in the linear regime, for compatibility with the reverberation room tests.

The portable meter was used both with a sample holder, and non-destructively, by screwing the sample holder or the flange onto the end of the tube. The flange used for the test panels was flat, though it may be curved to fit any given surface contour. The acoustic centre task was performed before the sample holder or flange was used, to ensure the distance to the sample surface was updated accordingly.

Test materials

A locally reacting material is one where the acoustic impedance at a point on the surface is independent of the angle of the incident sound. Typical examples are resistive sheets backed by relatively narrow cavities made from honeycomb cells, such as those used for aircraft engine nacelle ducts. In these materials only plane waves may propagate inside the panel at the design frequencies, up and down the individual honeycomb cells. Typical non-locally reacting materials include porous materials, mufflers with large acoustic cavities, and aircraft engine acoustic panels whose honeycomb cells are slotted for fluid drainage. Tests were performed here on both types of materials in order to compare the normal incidence flanged meter performance with that of the sample holder method, and with the random incidence reverberation room method.

The test panels, shown in Fig. 3, were as follows:

- Non-locally reacting – 11.3 m² Ecophon ceiling panels, with a 200 mm overall depth of system
- Locally reacting – 1.4 m² Diehl Aircabin single layer, 10 mm deep perforate panels, with 3.2 mm wide honeycomb core

In order to utilize the full eight square Ecophon panels in a uniform (rectangular) layout, they had an aspect ratio of approximately 0.5:1, slightly below the ISO 1 target of 0.7:1. Also, the available single layer perforate panel area fell well below the ISO 1 target of 10 to 12 m². However, the locally reacting panels were efficient enough to provide an equivalent absorption area change of more than 1 m² between 1000 and 3150 Hz.

Each panel was tested in the reverberation room, with the flanged impedance tube, and with samples cut to fit the 29 mm impedance tube sample holder.

Fig. 3. Non-locally reacting (left), and locally reacting (right), test panels



Results

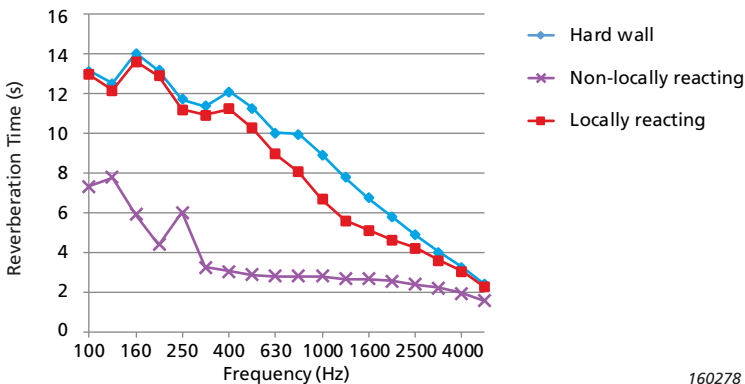
Reverberation Room Results

A fixed combination of microphone/source locations was used for the hard wall measurement and for the two lined measurements. The ambient conditions showed negligible variation of the measurements, so the same hard wall measurement was used for the calculation of absorption coefficient for each panel type.

Fig. 4 presents the measured reverberation times at 1/3-octave frequencies between 100 and 5000 Hz. While the large area (11.3 m²), non-locally reacting panel significantly reduces reverberation time at most frequencies, the relatively small area (1.4 m²), locally reacting panel provides a smaller impact, peaking at around 1 to 1.6 kHz.

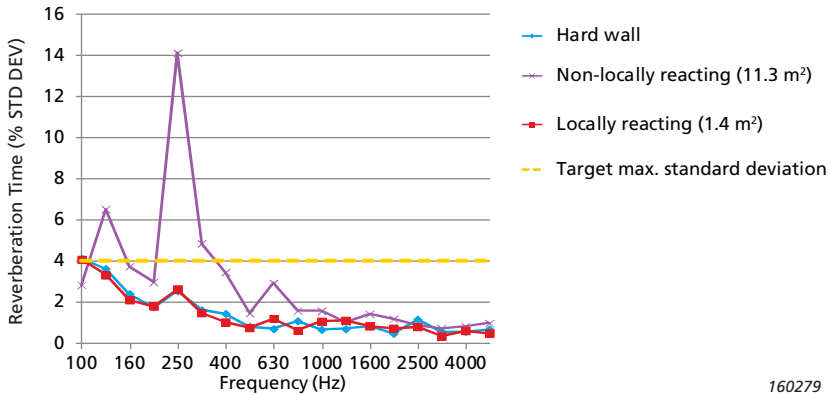
Fig. 5 shows the corresponding percentage standard deviation (standard deviation of 12 measurements from combinations of three source and four microphone locations, and with ten averages per combination). These are compared with a nominal limit standard deviation of 10% [17]. The plot shows that the standard deviation of the measured reverberation times is good for the locally reacting panel. The standard deviation for the non-locally reacting panel is generally only good for frequencies above 315 Hz. This is likely due to the existence of 2D modes which are not well attenuated for this panel [17]. The existence of these poorly attenuated modes is evidenced by some double slope decay curves at low frequencies, with a shorter decay time for 3D modes and a longer decay time for some 2D modes, for microphone and source locations most distant from the test panel.

Fig. 4. Measured reverberation times



160278

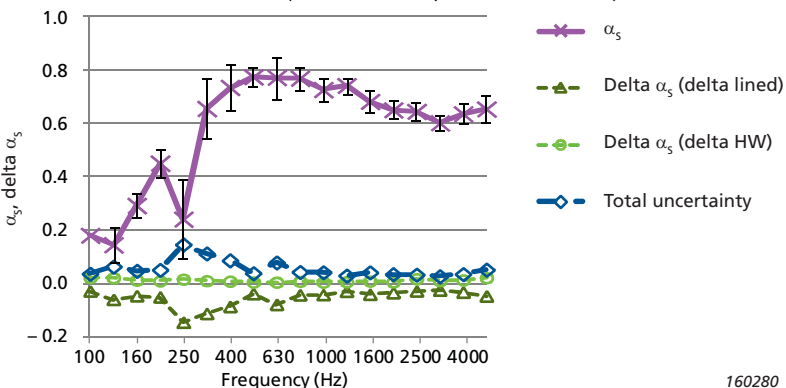
Fig. 5. Reverberation time percentage standard deviation



160279

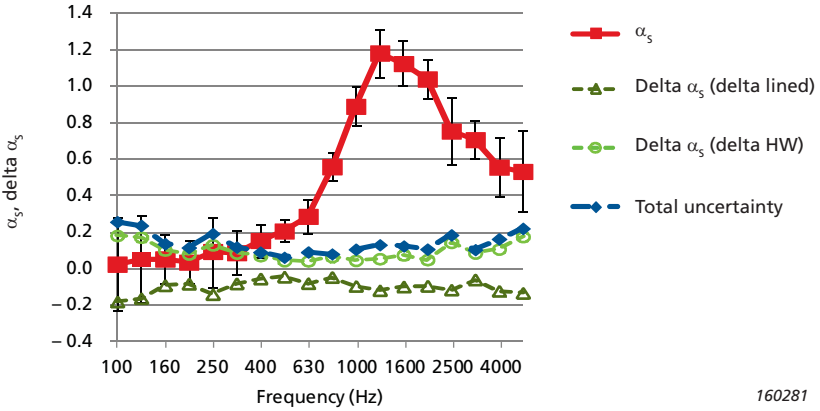
Fig. 6 and Fig. 7 show the measured absorption coefficient for the two panels, along with the uncertainty due to the variation in reverberation time measurements. As expected, the non-locally reacting panel absorption coefficient spectrum is more broadband, while the single layer locally reacting panel is more narrowband. The locally reacting panel data shows absorption coefficients greater than 1. This is most likely due to edge diffraction, where the apparent panel area is greater than the physical area, particularly for panels with a relatively high perimeter to area ratio [13, 14]. It is noted that this is a phenomenon which cannot occur for a normal incidence impedance tube measurement, where the absorption coefficient must be between 0 and 1.

Fig. 6. Non-locally reacting panel; sound absorption coefficient, α_s , and uncertainty due to reverberation time standard deviation (12 source/microphone combinations)



160280

Fig. 7. Locally reacting panel; sound absorption coefficient, α_s , and uncertainty due to reverberation time standard deviation (12 source/microphone combinations)



160281

Equation 1 was differentiated with respect to the measured reverberation times T_1 and T_2 in order to assess the influence of the standard deviation in the measured decay time on the calculated absorption coefficient, α_s . Assuming constant speeds of sound and constant atmospheric absorption for the hard wall and lined measurements, the uncertainty in α_s due to the reverberation time uncertainty, and the subsequent root sum square uncertainty, is given by

$$\delta\alpha_s(HW) = \left[\frac{-55.3V}{cS} \right] \left(\frac{\delta T_2}{T_2^2} \right) \quad (5)$$

$$\delta\alpha_s(Lined) = \left[\frac{55.3V}{cS} \right] \left(\frac{\delta T_1}{T_1^2} \right) \quad (6)$$

$$\delta\alpha_s(Root\ Sum\ Square) = \left[\frac{55.3V}{cS} \right] \left\{ \left(\frac{\delta T_2}{T_2^2} \right)^2 + \left(\frac{\delta T_1}{T_1^2} \right)^2 \right\}^{0.5} \quad (7)$$

Fig. 6 shows an approximate uncertainty in α_s of ± 0.1 at low frequency, reducing to around ± 0.04 at high frequency, for the 11.3 m^2 non-locally reacting panel. The minimum root sum square uncertainty for the 1.4 m^2 locally reacting panel is ± 0.05 and generally between ± 0.10 and ± 0.20 . The uncertainty in α_s arising from the hard wall measurements is higher for the smaller area of the

locally reacting panel, than for the non-locally reacting panel, due to the $1/S$ term in Equation 5.

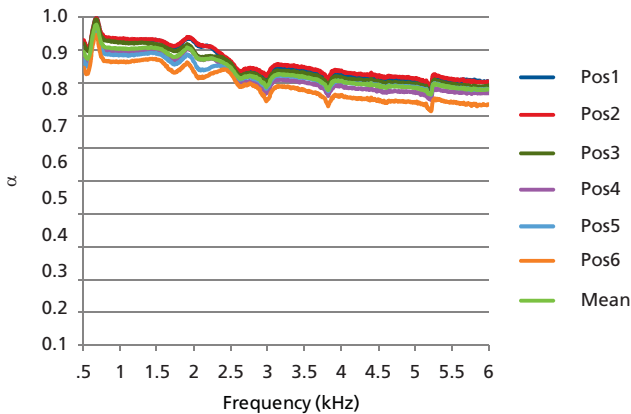
The reverberation room has the benefit of providing absorption coefficient results at random incidence. Uncertainties result from reverberation time differences for varying source/microphone locations, and from variations in edge diffraction for panels with differing perimeter to area ratios. It is noted that the measured uncertainty in sound absorption coefficient due to reverberation time uncertainty is increased in these test cases relative to that for ideal test conditions due to the non-perfectly diffuse room conditions, and the small locally reacting panel size.

The reverberation room measurement is also relatively time consuming. The portable impedance tube, however, provides rapid measurements of absorption coefficient and impedance, in much reduced time. One drawback of the impedance tube is that it can only measure normal incidence results. However, results for locally reacting panels may be corrected for random incidence using Fahy's method. The next section reports on the corresponding flanged impedance tube measurements.

Flanged Impedance Tube Results

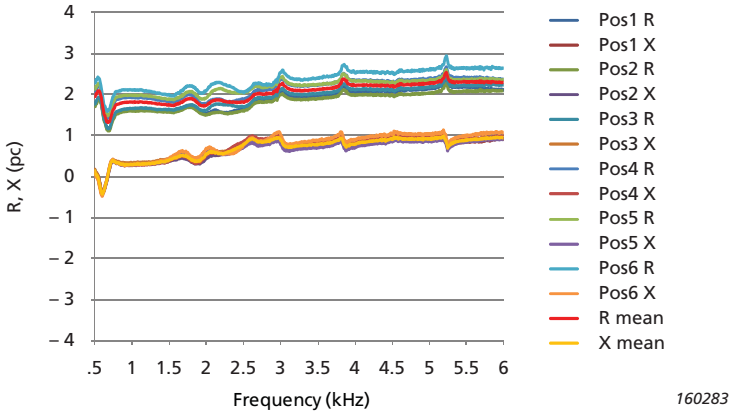
The impedance meter provides a more direct means of measurement of absorption coefficient. The meter is also portable, and measurements are very fast (less than one minute typically per test location). Fig. 8 to Fig. 11 show the flanged impedance tube normal incidence absorption coefficient and impedance

Fig. 8. Non-locally reacting panel: flanged impedance tube, normal incidence sound absorption coefficient, α



160282

Fig. 9. Non-locally reacting panel: flanged impedance tube, normal incidence impedance



for the test panels. Measurements were performed at a surface OASPL of 120 dB. The 29 mm inner diameter tube measurements were made over a number of locations for each panel type. As the method is non-destructive, the repeatability at a fixed location is excellent (not shown). Hence, the repeatability and reproducibility is much better than the Kundt tube with a sample holder (see Table 2 of Reference [3]).

As stated earlier, one of the advantages of the impedance meter is that it measures impedance in addition to absorption. Looking at the impedance curves

Fig. 10. Locally reacting panel: flanged impedance tube, normal incidence sound absorption coefficient, α

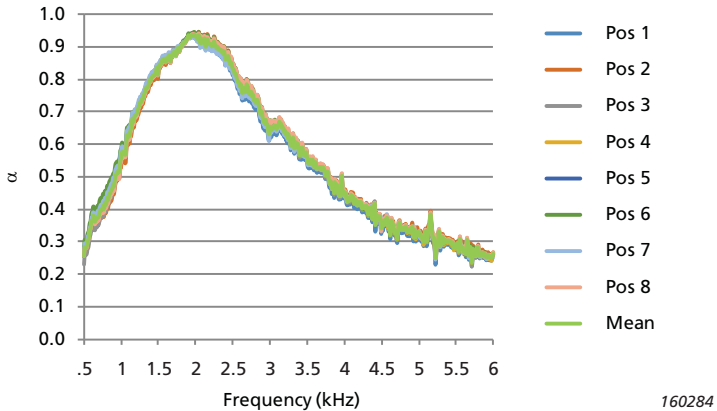
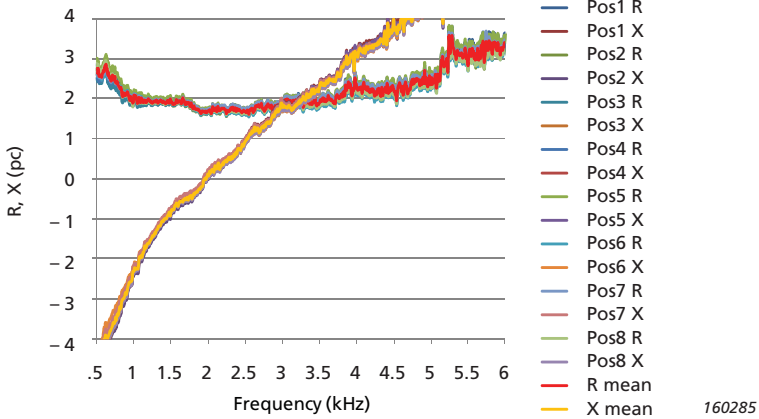


Fig. 11. Locally reacting panel: flanged impedance tube normal incidence impedance



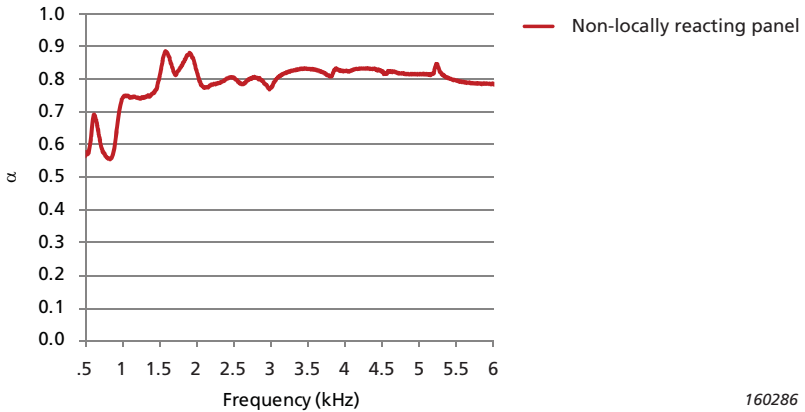
allows a designer to evaluate the panel resistive and reactive components. For example, the normal incidence absorption at the peak frequency may be increased via a reduction in resistivity (resistance per unit thickness) or material thickness for the non-locally reacting panels, or through a reduction in facing sheet resistance for the perforate panel. Also, sample holder tests on samples with reduced thicknesses of resistive material (not shown) demonstrated that “blips” in the spectra are due to quite heavily damped reactance oscillations for the 200 mm ODS (overall depth of system) installation. These oscillations are less damped for shallower thicknesses of the absorptive material.

Sample Holder Impedance Tube Results

Fig. 12 to Fig. 15 show the equivalent measurements for samples cut from the large test panels, to fit inside the 29 mm inner diameter sample holder. While the non-locally reacting panel material was relatively straightforward to cut to size and seal at the tube inner walls, the single layer perforate panel, with a facing sheet plus honeycomb core construction, was more difficult to cut to size. As a result, tests were repeated with plasticine to seal around the edges of the facing sheet.

The results for the non-locally reacting panel are consistent between the sample holder (Fig. 12, Fig. 13) and the flanged tube (Fig. 8, Fig. 9) for frequencies above 2000 Hz. The results diverge slightly at lower frequencies. This is due to a combination of the flange effect (mismatch between tube area and “visible” area of the sample [18]) and the non-locally reacting nature of the material; both effects are greatest at low frequencies.

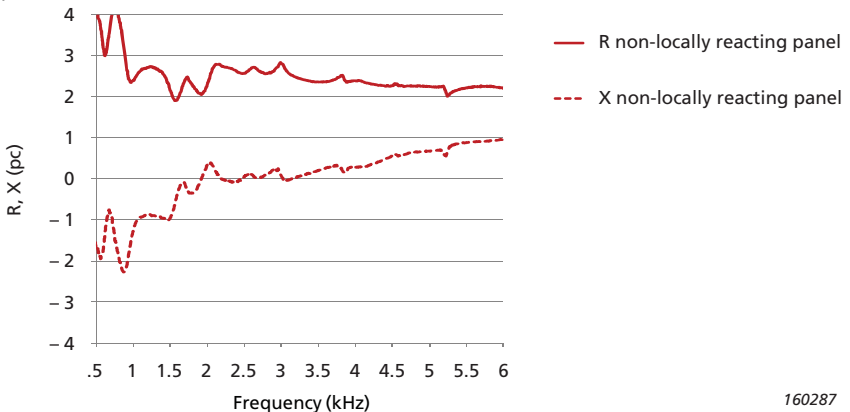
Fig. 12. Non-locally reacting panel: impedance tube sample holder, normal incidence sound absorption coefficient, α



160286

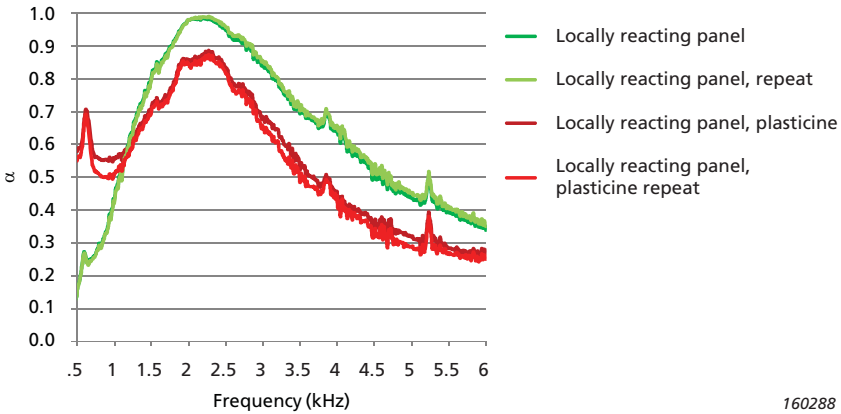
The combination of poor sealing and the plasticine absorption lead to very different results for the locally reacting panel tests inside the sample holder. The difficulty in cutting the facing sheet leads to unacceptable repeatability (see targets in Table 2 of Reference [3]). However, the mean of these results lie quite close to the flanged tube results. It is noted that Reference [19] provides guidance for obtaining the best possible sample mounting in an impedance tube sample holder.

Fig. 13. Non-locally reacting panel: impedance tube sample holder, normal incidence impedance



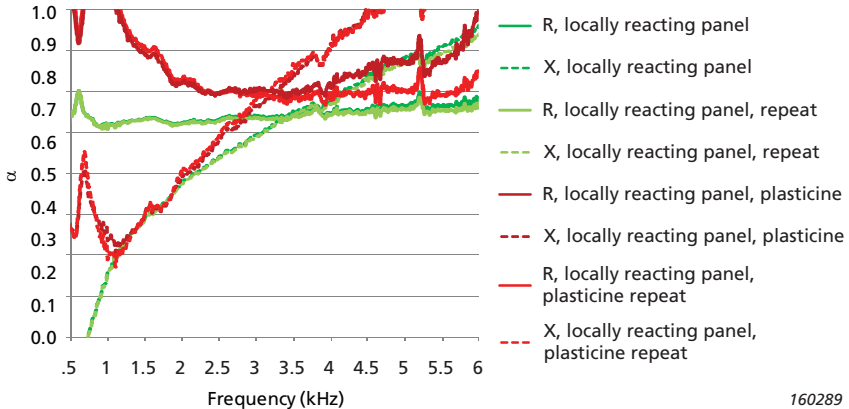
160287

Fig. 14. Locally reacting panel: impedance tube sample holder, normal incidence sound absorption coefficient, α



160288

Fig. 15. Locally reacting panel. Impedance tube sample holder normal incidence impedance



160289

Comparison of Flanged Impedance Tube and Reverberation Room Measurements

The sample holder tests highlighted the advantages and disadvantages of the sample holder. The advantages include the tube area equalling the sample area, and the sample being forced to be locally reacting, giving more controlled conditions at low frequencies. The disadvantages are that some samples are difficult to cut and seal inside the holder, and that the tests are destructive.

In order to compare the flanged impedance tube results with the reverberation room measurements more directly, the flanged tube results were corrected for random incidence using Fahy's equation [16]. Fahy derived a relationship between the normal incidence impedance and the random incidence absorption coefficient ($\alpha_{Diffuse}$) for a locally reacting material, where $\alpha_{Diffuse}$ is given by

$$\alpha_{Diffuse} = 8\Gamma \left\{ 1 - \Gamma \ln \left[\frac{r}{\Gamma} + 2r + 1 \right] + \frac{x}{r} \Gamma \left[\left(\frac{r}{x} \right)^2 - 1 \right] \tan^{-1} \left[\frac{x}{r+1} \right] \right\} \quad (8)$$

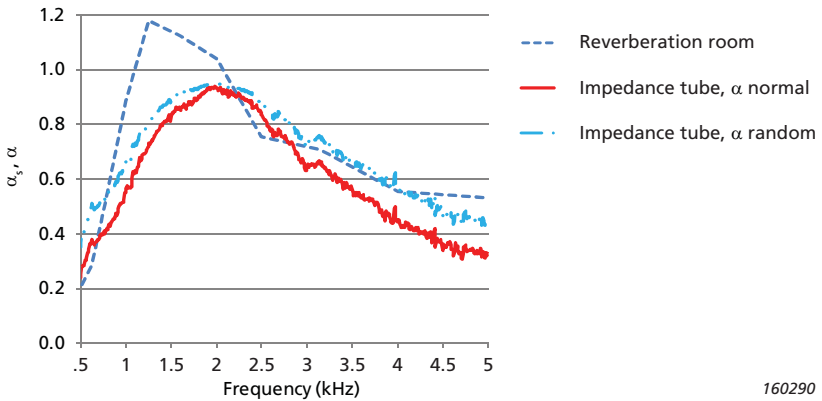
where R and X are real imaginary components of normal incidence impedance Z, and $\Gamma = (R^2 + X^2)^{1/2}$.

Fig. 16 and Fig. 17 show absorption coefficient comparisons between the reverberation room measurements and the flanged impedance tube measurements, for the locally reacting and the non-locally reacting materials.

The flanged impedance tube normal incidence absorption coefficient is shown, along with the diffuse field value. In both cases, the diffuse field value is higher than the normal incidence value.

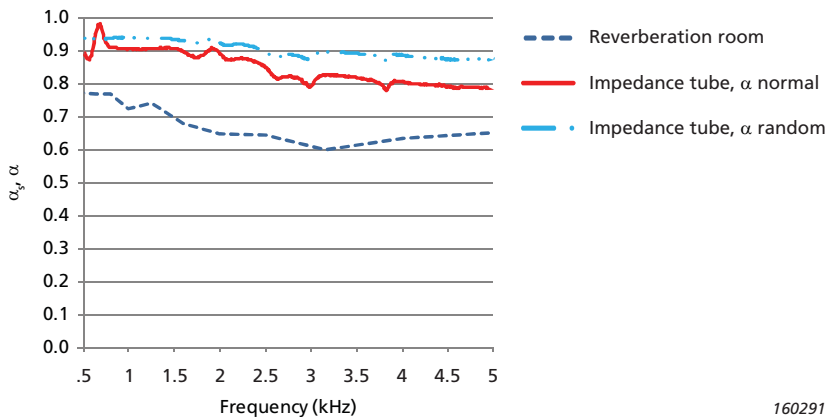
The diffuse field absorption coefficient and the reverberation room absorption coefficient results for the locally reacting panel (Fig. 16) show excellent agreement for frequencies above 2 kHz. Below this frequency, the reverberation room results exceed unity. This is likely due to edge diffraction. The diffuse field impedance tube results are expected to be good for this panel at low frequencies,

Fig. 16. Locally reacting panel comparison of reverberation room and flanged impedance tube absorption coefficient measurements



160290

Fig. 17. Non-locally reacting panel comparison of reverberation room and flanged impedance tube absorption coefficient measurements



160291

as the relatively narrow panel core width of 3.2 mm minimizes the ratio of the tube area to “visible” sample area.

The comparison for the non-locally reacting panel (Fig. 17) show larger differences between the diffuse field impedance tube results and the large panel reverberation room results. The maximum delta of approximately 0.2 exceeds the test reverberation room uncertainty due to reverberation time uncertainty. The reverberation room absorption coefficient lies below that from the impedance meter, though the shape of the curves are similar.

Some cross-checks were made on the Brüel & Kjær reverberation room results. Results measured at a different reverberation room for the locally reacting panel, showed excellent agreement with the Brüel & Kjær data. The reason for the larger discrepancy for the non-locally reacting panel may be due to non-perfectly diffuse field conditions and/or sensitivity to the panel location.

Further work is recommended to investigate the sensitivity of the reverberation room measurements to the level of diffusivity of the Brüel & Kjær test room (as this has not been investigated), panel installation (for example, grouped versus individual panels), panel orientation and panel location. Reference [15] points to the “remarkable” increase in measured absorption coefficient when additional diffusers were added to the reverberation test room. The same reference also highlights the impact of panel orientation, with high absorption coefficients being measured for panel orientations non-parallel to the reverberation room walls.

Conclusions and Recommendations

This paper has described a method of performing in situ testing of panel absorption and impedance characteristics, using a flanged Kundt tube arrangement. Absorption coefficient and impedance measurements were made on non-locally reacting and locally reacting materials. Results were compared with absorption measurements made using the reverberation room method, and the impedance tube sample holder method.

The portable flanged impedance tube was shown to be quicker, simpler, and more repeatable than both reverberation room and sample holder impedance tube tests. This non-destructive procedure may be used in situ to measure panels in the installed condition. Furthermore, the measurement of impedance, in addition to absorption coefficient, provides key additional information which may be used to help designers re-tune a given panel installation for improved performance.

Each of the methods compared have their pros and cons. The reverberation room method measures the absorption coefficient at random incidence. The uncertainty in absorption is a strong function of the standard deviation of the measured reverberation times, while differences in panel perimeter-to-area ratio lead to differing levels of edge diffraction. Impedance tube tests performed using a sample holder suffer for materials which are difficult to cut and seal in the tube.

Flanged tube absorption coefficient measurements for high resistivity, non-locally reacting panels, or for locally reacting panels, may be corrected for random incidence performance using Fahy's method. Measurements for highly non-locally reacting materials are most reliable at higher frequencies, as for lower frequencies, some of the incident sound not absorbed locally, and not reflected back up the tube, propagates laterally through the test material. It is noted that the Brüel & Kjær tube software can apply a factor to convert flanged tube results to the equivalent sample holder result. This may be derived by making flanged measurements, and comparing them with sample holder measurements made using well prepared samples.

It is recommended that additional flanged impedance tube measurements are made for non-locally reacting materials of both lower and higher resistivity than that tested, and for absorbers with air gaps behind them. Furthermore, comparisons with the PU probe would help identify the strengths and weaknesses of both of these in situ methods.

References

- [1] ASTM C423-09a. “Standard Test Method for Sound Absorption and Sound Absorption Coefficients by the Reverberation Room Method.”
- [2] ISO 354:2003. “Acoustics - Measurement of sound absorption in a reverberation room.”
- [3] ASTM E1050-12. “Standard Test Method for Impedance and Absorption of Acoustical Materials using a Tube, Two Microphones, and a Digital Frequency analysis System.”
- [4] ISO 10534-2. “Acoustics - Determination of sound absorption coefficient and impedance in impedance tubes - Part 2: Transfer- function method.”
- [5] Kunio, J., Yoo, T., Hoo, K. and Enok, J. “A Comparison of Two and Four Microphone Standing Wave Tube Procedures for Estimating the Normal Incidence Absorption Coefficient.” *Internoise*, August 2009.
- [6] CEN/TS 1793-5:2003. “Road traffic noise reducing devices – Testing method for determining the acoustic performance – Part 5: Intrinsic Characteristics – In situ values of sound reflection and airborne sound insulation.”
- [7] Tijs, E. and Druyvesteyn, E. “An Intensity Method for Measuring Absorption Properties in situ”, *ACTA ACUSTICA*, Vol. 98 (2012).
- [8] Jambrošić, K., Suhaneč, M. and Petošić, A. “Comparison of two methods for in-situ measurement of the absorption coefficient.” *EURONOISE*, October 2009.
- [9] Barnard, A. R. and Rao, M. D. “A Comparison of Acoustic Absorption Coefficient Measurements from the In-Situ Method with Traditional Methods”, *NOISE-CON*, July 2004.
- [10] Cats, P., Tijs, E. and Comesana, D. F. “Exploration of the differences between a pressure-velocity based in situ absorption measurement method and the standardized reverberant room method.” *ICA*, June 2013, paper 5aAAb3.
- [11] Ramis, J., Alba, J., Martínez, J. and Redondo, J. “The uncertainty in absorption coefficients measured in reverberant chambers: A case study”, *NVWW*, Jan. 2005.

- [12] Texier, M.L. and Betjemann, P. “An estimation of the measurement uncertainties of the sound absorption coefficient.” Eurnoise, 2009.
- [13] Sauro, R., Vargas, M. and Mange, G. “Absorption coefficients – part 1: is square area enough?” Internoise, August 2009.
- [14] Sauro, R., Vargas, M. and Mange, G. “Absorption coefficients- part 2: is “edge effect” more important than expected?” Internoise, August 2009.
- [15] D’Alessandro, F. and Pispola, G. “Sound absorption properties of sustainable fibrous materials in an enhanced reverberation room”, Internoise, August 2005.
- [16] Fahy, F. “Foundations of Engineering Acoustics”, Chapter 7. Academic Press, 2001.
- [17] Rindel, J. H. “ODEON – Non diffuse room example.” Online document. Odeon A/S, Scion DTU, Denmark. 18.
- [18] Murray, P. B., Ferrante, P. and Scofano, A. “The Influence of Aircraft Nacelle Acoustic Panel Drainage Slots on Duct Attenuation”, AIAA, 2007-3548.
- [19] Stanley, D. R. “Impedance Tube Specimen Preparation and Mounting Issues.” Internoise, August 2012.
- [20] Gramtorp, J. Unpublished data, Brüel & Kjær, 2014.

Contact Information

Paul Murray is an Acoustic Consultant with Morrisbrand Ltd in Horsham, W. Sussex, UK. Email: paulbmurray@morrisbrand.co.uk

Jason Kunio INCE Bd. Cert. is an Application Engineer with Brüel & Kjær North America in Chicago. Email: Jason.Kunio@bksv.com

Flemming Schultz Larsen is an Aerospace and Defence Strategic Marketing Manager with Brüel & Kjær Denmark. Email: Flemming.Larsen@bksv.com

Acknowledgements

The authors would like to acknowledge Max Falck and colleagues of Ecophon, Denmark, and Jens Muller and colleagues of Diehl Aircabin, Germany, who kindly supplied the test panels. They would also like to thank Noel Brown and Flemming Nielsen of Brüel & Kjær Sound & Vibration Measurement A/S for their help in arranging the tests.

Previously issued numbers of Brüel & Kjær Technical Review

(Continued from cover page 2)

- 1 – 2002 A New Design Principle for Triaxial Piezoelectric Accelerometers
Use of FE Models in the Optimisation of Accelerometer Designs
System for Measurement of Microphone Distortion and Linearity from
Medium to Very High Levels
- 1 – 2001 The Influence of Environmental Conditions on the Pressure Sensitivity of
Measurement Microphones
Reduction of Heat Conduction Error in Microphone Pressure Reciprocity
Calibration
Frequency Response for Measurement Microphones – a Question of
Confidence
Measurement of Microphone Random-incidence and Pressure-field
Responses and Determination of their Uncertainties
- 1 – 2000 Non-stationary STSF
- 1 – 1999 Characteristics of the vold-Kalman Order Tracking Filter
- 1 – 1998 Danish Primary Laboratory of Acoustics (DPLA) as Part of the National
Metrology Organisation
Pressure Reciprocity Calibration – Instrumentation, Results and Uncertainty
MP.EXE, a Calculation Program for Pressure Reciprocity Calibration of
Microphones
- 1 – 1997 A New Design Principle for Triaxial Piezoelectric Accelerometers
A Simple QC Test for Knock Sensors
Torsional Operational Deflection Shapes (TODS) Measurements
- 2 – 1996 Non-stationary Signal Analysis using Wavelet Transform, Short-time
Fourier Transform and Wigner-Ville Distribution
- 1 – 1996 Calibration Uncertainties & Distortion of Microphones.
Wide Band Intensity Probe. Accelerometer Mounted Resonance Test
- 2 – 1995 Order Tracking Analysis

Special technical literature

Brüel & Kjær publishes a variety of technical literature that can be obtained from your local Brüel & Kjær representative.

The following literature is presently available:

- Catalogues
- Product Data Sheets

Furthermore, back copies of the Technical Review can be supplied as listed above. Older issues may be obtained provided they are still in stock.

Front cover: Neuburg airfield, Germany

Each Brüel & Kjær Technical Review contains a collection of technical, scientific articles that describe theory, measurement techniques and instrumentation, which are specifically aimed at acousticians and vibration engineers.

See more on bksv.com/Knowledge-center, Technical Reviews

